Mechanical Exfoliation and Characterization of Single- and Few-Layer Nanosheets of WSe_2, TaS_2, and $TaSe_2$

Hai Li, Gang Lu, Yanlong Wang, Zongyou Yin, Chunxiao Cong, Qiyuan He, Lu Wang, Feng Ding, Ting Yu, and Hua Zhang**

Single- and few-layer transition-metal dichalcogenide nanosheets, such as WSe_2, TaS_2, and $TaSe_2$, are prepared by mechanical exfoliation. A Raman microscope is employed to characterize the single-layer (1L) to quinary-layer (5L) WSe_2 nanosheets and WSe_2 single crystals with a laser excitation power ranging from 20 μW to 5.1 mW. Typical first-order together with some second-order and combinational Raman modes are observed. A new peak at around 308 cm^{-1} is observed in WSe_2 except for the 1L WSe_2, which might arise from interlayer interactions. Red shifting of the A_{1g} mode and the Raman peak around 308 cm^{-1} is observed from 1L to 5L WSe_2. Interestingly, hexagonal- and monoclinic-structured WO_3 thin films are obtained during the local oxidation of thinner (1L–3L) and thicker (4L and 5L) WSe_2 nanosheets, while laser-burned holes are found during the local oxidation of the WSe_2 single crystal. In addition, the characterization of TaS_2 and $TaSe_2$ thin layers is also conducted.

1. Introduction

In recent years, two-dimentional (2D) layered nanomaterials have attracted much attention due to their unusual physical properties.[1–16] For example, graphene, a single-layer 2D carbon material with honeycomb lattice structure, is the most widely studied 2D nanomaterial owing to its exceptional electronic, optical, thermal, and mechanical properties.[4,5] Other 2D layered inorganic graphene analogues, such as transition-metal dichalcogenides (TMD, e.g. MoS_2,[2,6–10,14–19] WS_2,[9,10,16,19] ZrS_2,[9] $MoSe_2$,[10] $NbSe_2$,[10,14,20] TiS_2,[9] TaS_2,[9] and WSe_2[14,21–24]), are also important and have been extensively exploited in the fields of lubrication, catalysis, energy storage, electronics and sensors.[2,6–15,17–19,21–24] These TMD materials consist of the hexagonal layer of metal atoms (*M*) sandwiched between two layers of chalcogen atoms (*X*) with a common formula of MX_2. There is strong covalent bonding in the hexagonal layer and weak van der Waals (vdW) interaction between the adjacent layers.

Recently, as a typical example of semiconducting TMD, MoS_2 has attracted significant research interest and shows many interesting applications.[2,6–15,17,19] As another kind of TMD materials, WSe_2 gives the wide photovoltaic application in the conversion of solar energy into electricity, due to its high absorption coefficient in the visible and near-infrared regions of spectrum and excellent output stability as photoelectrodes.[21,25–32] Lots of efforts focused on the photoelectrochemical etching of WSe_2 crystal to improve its photoresponse.[26–30,32] It was generally accepted that the quality of exposed vdW surface of WSe_2 can significantly affect the conversion efficiency from the solar energy to electricity.[26,27,30] Therefore, a careful cleavage of the

Dr. H. Li, Dr. G. Lu, Dr. Z. Yin, Q. He, Prof. H. Zhang
School of Materials Science and Engineering
Nanyang Technological University
50 Nanyang Avenue, Singapore 639798, Singapore
Website: http://www.ntu.edu.sg/home/hzhang/
Phone: +65-6790-5175; Fax: +65-6790-9081
E-mail: hzhang@ntu.edu.sg
Y. Wang, Dr. C. Cong, Prof. T. Yu
Division of Physics and Applied Physics
School of Physical & Mathematical Sciences
Nanyang Technological University
21 Nanyang Link, Singapore 637371, Singapore
E-mail: YuTing@ntu.edu.sg
Dr. L. Wang, Prof. F. Ding
Institute of Textiles and Clothing
Hong Kong Polytechnic University
Kowloon, Hong Kong, China

DOI: 10.1002/smll.201202919

NANO MICRO small

vdW face of WSe_2 is essential to achieve the high conversion efficiency.[27]

It has been reported that the physical and electronic properties of 2D layered nanomaterials are highly related to their thickness.[1,2,4–7,11–15,21–23,33,34] Recently, the ultralow cross-plane thermal conductivity (0.05 W/mK) and low in-plane thermal conductivity (1.2–1.6 W/mK) have been found in the layered WSe_2 thin films.[21–24] Therefore, a uniform and defect-free WSe_2 thin film is highly desirable. Moreover, it is reported that the mechanical control plays an important role on the nanomaterials and nanosystems.[35] To date, the scotch tape-based mechanical cleavage is the easiest and fastest way to obtain the pristine, highly crystalline, atomically-thin layers of 2D nanomaterials, such as graphene, MoS_2, $NbSe_2$, WSe_2, and topological insulators (e.g. Bi_2Te_3, Bi_2Se_3, and Sb_2Te_3).[1–8,11–15,33,34,36,37] It enables the direct investigation of the intrinsic properties of 2D layered nanomaterials.

Many methods have been well established to characterize the 2D layered nanomaterials, such as the scanning probe microscopy (SPM),[6] scanning electron microscopy (SEM),[36] transmission electron microscopy (TEM),[9,10,17] Raman spectroscopy, and optical microscopy (OM).[7,14,33,38–40] Among them, Raman spectroscopy is a powerful and sensitive technique for the rapid identification and characterization of 2D layered nanomaterials.[12,34,37–39,41] Although Raman spectroscopy is widely used to characterize the stable 2D nanomaterials, such as graphene and MoS_2, the localized laser-induced heating may damage those materials with low melting points.[33,34,36,37] It has been reported that the laser excitation power above 0.5 mW can generate holes on Bi_2Te_3.[33] The similar phenomenon was also observed on Bi_2Se_3 and hence Raman microscope with laser excitation power as low as 70 μW was used to characterize Bi_2Se_3.[34] To date, only few reports focused on the Raman characterization of bulk single crystal of WSe_2 possibly due to the easy damage of WSe_2 by the laser-induced heating.[25,42] To the best of our knowledge, there is no systematic characterization of single- to few-layer WSe_2 nanosheets and WSe_2 single crystal by Raman spectroscopy with the suitable laser excitation power.

Herein, single- (1L) to quinary-layer (5L) TMD nanosheets, such as WSe_2, TaS_2, and $TaSe_2$, were prepared on Si/SiO_2 substrates by the mechanical exfoliation. Raman microscope with the 532 nm laser was employed to characterize the 1L to 5L WSe_2 nanosheets and the WSe_2 single crystal with the laser excitation power varying from 20 μW to 5.1 mW. The typical first order Raman peaks together with some second order and the combinational modes were observed. A new Raman peak at 308 cm^{-1} was observed in the spectra of WSe_2 except for the 1L WSe_2 nanosheet, which might arise from the interlayer interaction. As the layer number increased from 1L to 5L, red shift of the A_{1g} mode and the Raman peak around 308 cm^{-1} was observed. In addition, the high power laser-induced local oxidation of thin-layer WSe_2 nanosheets and WSe_2 single crystal was monitored by Raman spectroscopy and atomic force microscopy (AFM). After oxidation, the formed nanostructures with 60° or 120° angle at edges were observed in the 1L to 3L WSe_2 nanosheets, while the burned holes were found in the WSe_2 single crystal. Moreover, few-layer TaS_2 and $TaSe_2$ nanosheets were also prepared by the mechanical exfoliation method and subsequently characterized by OM and AFM.

2. Results and Discussion

Recently, Teweldebrhan et al. found that the 488 nm laser with excitation power higher than 0.5 mW could damage Bi_2Te_3, which has a low melting point of 573 °C, due to the local melting or oxidation.[33] Since the bulk WSe_2 has a melting point of 800 °C,[43] the laser-induced local heating might also damage WSe_2. It is very important to get the suitable laser excitation power for the Raman measurement to exclude any destructive laser heating effect.

In order to have a reference of the characteristic Raman peaks and optimize the laser power, a WSe_2 single crystal was investigated with the 532 nm laser at different excitation powers. As known, the 2H-WSe_2 (D^4_{6h}) possesses 12 zone centre lattice vibrational modes. Among them, four modes (E^2_{2g}, E_{1g}, E^1_{2g} and A_{1g}) are Raman active (**Figure 1**A).[25] As shown in Figure S1A in the Supporting Information (SI), no well-resolved Raman peak was observed with the laser power of 43 μW. Raman spectrum with good signal-to-noise (S/N) ratio was achieved when the laser power was increased to 0.28 mW (Figure 1B and Figure S1A in SI). There are two strong peaks with similar intensity at 247 and 257 cm^{-1}, which can be assigned to E^1_{2g} and A_{1g} modes,[25] respectively. Raman spectra with more featured Raman peaks were achieved when the laser power was further increased to 0.58 mW and 2.6 mW (Figure 1B). The other peaks observed in the range of 100–420 cm^{-1} are assigned as the second order and combinational modes,[44,45] which are listed in the Table S1. The broad weak peaks at 490, 510, 624 and 745 cm^{-1} were also observed in the spectral range of 450–900 cm^{-1} (Figure 1B and Figure S1B in SI), which could be the higher order overtones and combinational modes. Due to the limitation of our Raman spectroscope, we are not able to see the low frequency rigid-layer E^2_{2g} mode.[25] The E_{1g} mode cannot be observed either because this mode is Raman inactive for the normal incidence. In order to identify it, the detailed polarization study is required.[46,47]

When the excitation power was increased to 2.6 mW, the laser-induced formation of a 1.5 nm high film in WSe_2 single crystal, which might be the tungsten trioxide (WO_3) by considering our Raman measurements performed in the ambient conditions, was observed by AFM measurement (Figure 1D,E). However, no notable Raman signal of WO_3 was observed, which might be attributed to the insufficient amount of WO_3 for Raman characterization. When the excitation power was increased to 5.1 mW, similar to Bi_2Te_3,[33] the laser-burned hole with a depth of 96 nm appeared in the WSe_2 single crystal (Figure 1C,D) and the obvious Raman signal of monoclinic WO_3 was observed (Figure 1B). Two strong peaks at 707 and 804 cm^{-1} and a weak peak at 328 cm^{-1} were clearly observed in the Raman spectrum (Figure 1B), which are typical characteristics of monoclinic WO_3 (O-W-O stretching mode),[48–53] confirming the local oxidation induced by laser heating when the laser power is high.

After layered WSe_2 nanosheets were deposited on Si/SiO_2 by using the mechanical exfoliation method, OM and AFM were used to locate and identify the layer numbers. The properties of 1L to 5L WSe_2 nanosheets are different from that of the WSe_2 single crystal. Different from the bulk WSe_2, Raman spectra with acceptable peak features of 1L to 5L WSe_2

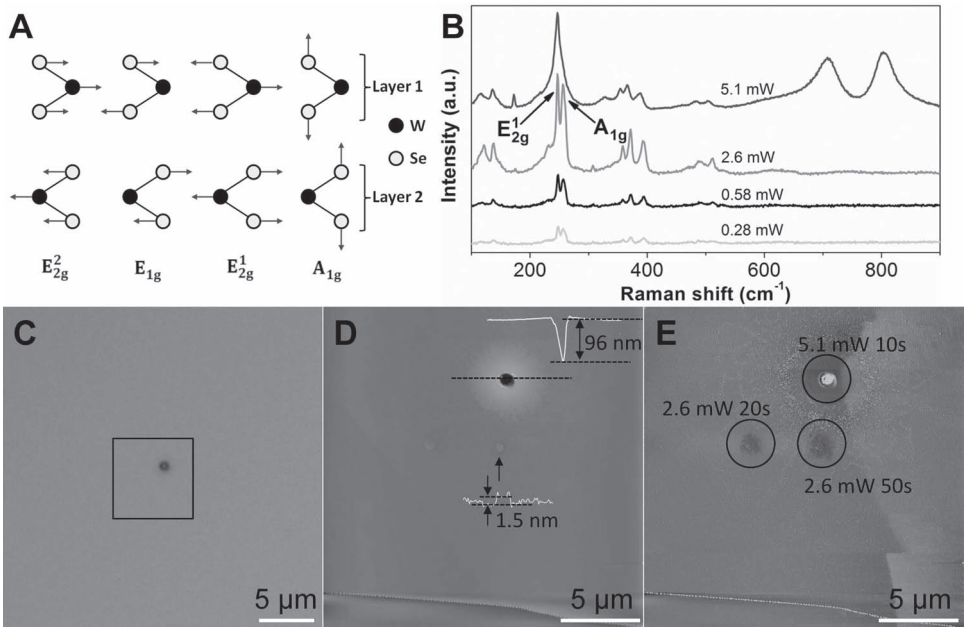

Figure 1. (A) Atomic displacements of the four Raman-active modes in the unit cell of the bulk WSe_2 crystal. (B) Raman spectra of WSe_2 single crystal when the laser excitation power was increased from 0.28 mW to 5.1 mW. (C) Optical image of WSe_2 single crystal after the Raman characterization. (D) AFM height and (E) phase images of the black square area in (C).

nanosheets were observed at an excitation power as low as 20 μW (Figure S2 in SI). Raman spectra with good S/N ratio were achieved when the excitation power was increased to 43 μW (**Figure 2**A–C). The strongest Raman spectrum arose from the 2L WSe_2 nanosheet and the spectra became weaker as the layer number increased from 2L to 5L (Figure 2A–C and Figure S2 in SI). There are two strong peaks in the range of 245-265 cm^{-1} for all samples, which can be assigned to E^1_{2g} and A_{1g} modes, respectively.[25] Compared to the similar peak intensity of E^1_{2g} and A_{1g} modes in the WSe_2 single crystal (Figure 1B), the E^1_{2g} mode exhibits higher peak intensity than does the A_{1g} mode in the 1L to 5L WSe_2 nanosheets (Figure 2B). Similar to the single crystal of WSe_2, six weaker peaks were also observed in 2L to 5L WSe_2 nanosheets in the range of 100–415 cm^{-1}, as shown in Figure 2A,C. However, only five weaker peaks appeared in this range for the 1L WSe_2 nanosheet besides the E^1_{2g} and A_{1g} modes. There is no notable peak around 308 cm^{-1} for 1L WSe_2 nanosheet even when the laser power was increased to 0.58 mW (Figure S2 in SI), implying that this mode becomes Raman active only in 2L and thicker WSe_2 nanosheets. The detailed position of these peaks in the range of 100–420 cm^{-1} is listed in Table S1 in SI. Interestingly, as the layer number of WSe_2 nanosheets increased from 1L to 5L, a red shift of the A_{1g} mode and Raman peak around 308 cm^{-1} was observed (Figure 2D,E), which could reflect the presence of additional interlayer interaction.[40]

In order to get the optimal laser power for WSe_2 nanosheet, OM and AFM were used to monitor the morphology change of 2L WSe_2 nanosheet before (**Figure 3**A) and after (Figure 3B) Raman characterization by using laser with excitation power increased from 20 μW to 5.1 mW. No notable morphology change was detected when the excitation power was lower than 0.28 mW (Figure 3C). When the excitation power was increased from 0.58 W to 5.1 mW, the clear morphology change of 2L WSe_2 nanosheet was observed by both OM and AFM measurements (Figure 3B,C). In the optical image (Figure 3B), it can be seen that a white spot appeared in the 2L WSe_2 nanosheet when the laser power was increased to 0.58 mW, which might arise from the local oxidation after Raman characterization. It was proved by the AFM measurement (height profile of white dashed line in Figure 3C), which showed the

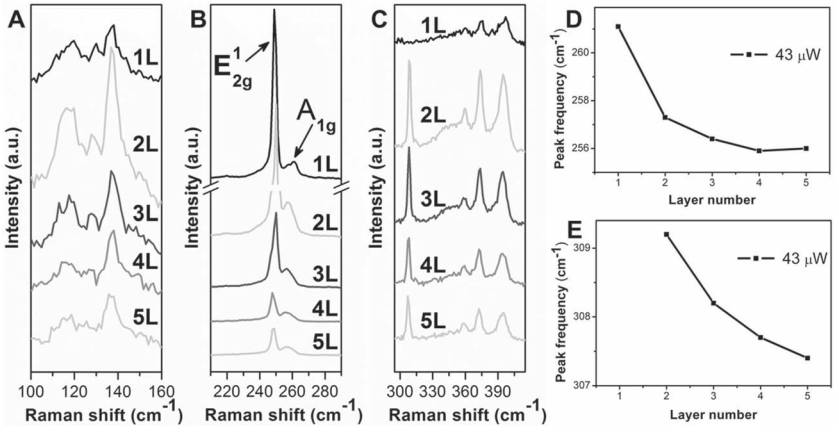

Figure 2. Raman spectra of 1L to 5L WSe_2 nanosheets at excitation power of 43 μW in the range of (A) 100–160 cm^{-1}, (B) 210–290 cm^{-1}, and (C) 295–415 cm^{-1}, respectively. (D–E) Peak frequencies of A_{1g} mode (D) and the Raman peak near 308 cm^{-1} (E) as a function of layer number of WSe_2 at excitation power of 43 μW.

small NANO MICRO

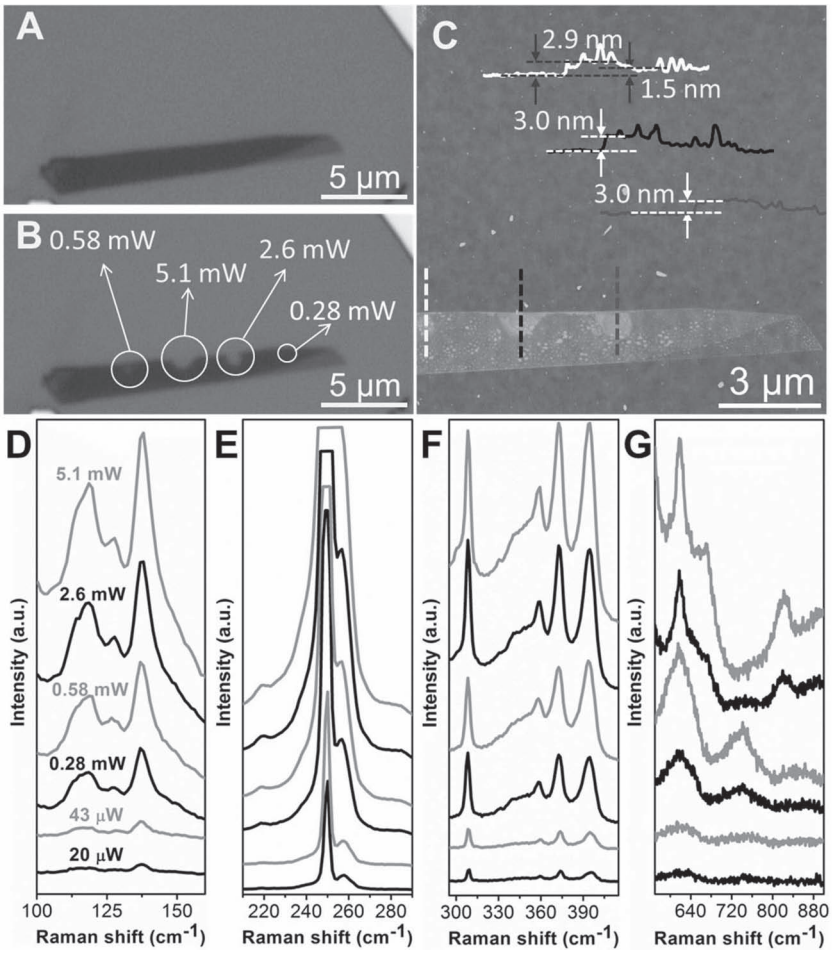

Figure 3. Optical images of 2L WSe_2 nanosheet before (A) and after (B) Raman characterization. The white circles in (B) show the spots where the Raman spectra were recorded. (C) The corresponding AFM image of the 2L WSe_2 nanosheet after Raman characterization in (B). Inset: height profiles of spots. (D-G) Raman spectra of 2L WSe_2 nanosheet in the range of (D) 100-160 cm^{-1}, (E) 210–290 cm^{-1}, (F) 295–415 cm^{-1}, and (G) 570–900 cm^{-1}, respectively, with laser excitation power increased from 20 μW to 5.1 mW. Note that the peak at 745 cm^{-1} disappeared and a new peak at 822 cm^{-1} appeared when the laser power was increased to 2.6 mW.

height of 2L WSe_2 nanosheet increased to ca. 2.9 nm after Raman characterization. When the laser power was further increased to 2.6 mW and then 5.1 mW, larger laser-induced oxidation spots were formed (Figure 3B,C). However, no notable change was observed in Raman spectra of 2L WSe_2 nanosheet in the range of 100–415 cm^{-1} even when the laser power was increased to 5.1 mW (Figure 3D–F). As shown in Figure 3G, the obvious changes were observed in the range of 570–900 cm^{-1} when the laser power was increased from 0.58 to 5.1 mW. The Raman peak of WSe_2 at 745 cm^{-1} disappeared after the 2L WSe2 nanosheet was exposed to laser with power higher than 0.58 mW for 10 s (Figure 3G). Meanwhile, a new weak peak appeared at 822 cm^{-1}, which can be attributed to the formation of the hexagonal WO_3.[48,52] Similar to the 2L WSe_2 nanosheet, as the excitation power was increased from 20 μW to 5.1 mW, the position and shape of all Raman peaks of 1L, and 3L to 5L WSe_2 nanosheets did not show pronounced changes in the range of 100–415 cm^{-1} (Figure S2 in SI). A new weak peak at 302 cm^{-1} appeared in the Raman spectrum of 1L WSe_2 nanosheet when the laser power was increased to 2.6 mW and then 5.1 mW (Figure S2I–L in SI), which was also observed in Raman spectra of 2L to 5L WSe_2 nanosheets and might be attributed to WO_3 arising from the high power laser-induced local oxidation.[54]

The Raman spectra of thin WSe_2 nanosheets are much stronger compared to the WSe_2 single crystal (Figure S3 in SI). Due to the weak Raman signal, Raman spectrum of WSe_2 single crystal at excitation power of 0.28 mW (Figure S3A,B in SI) and 0.58 mW (Figure S3C,D in SI) was accumulated for 5 times with 10 s for per accumulation. The remarkable enhancement of Raman peaks for 1L to 5L WSe_2 nanosheets could be due to the constructive interference of both excitation and scattering lights.[55]

In order to exploit the evolution of WSe_2 to WO_3 by the localized laser oxidation, 1L and 2L WSe_2 nanosheets were characterized by Raman spectroscopy repeatedly with an exposure time of 200 s and excitation power of 5.1 mW. **Figure 4**A,B and I-J show the optical images of 1L and 2L WSe_2 nanosheets before (Figure 4A: 1L; Figure 4I: 2L) and after (Figure 4B: 1L; Figure 4J: 2L) Raman characterization. As shown in Figure 4B and J, clear color difference on 1L and 2L WSe_2 nanosheets can be observed from optical images after exposure to laser with high power. The area exposed to laser is almost transparent (Figure 4B,J) and might be oxidized to form WO_3. AFM measurement indicates that the transparent area has a height of ~2 nm and brighter contrast than that of unexposed area as shown in height (Figure 4C,K) and phase images (Figure 4D,L). Interestingly, these transparent films have nanostructures with 60° or 120° angle at their edges (white arrows and dashed lines in Figure 4D,K, Figure S4 and S5 in SI), which might be hexagonal-structured WO_3. Especially for 2L WSe_2 nanosheet after oxidation (Figure S5 in SI), many triangle-shaped structures with a height of 2.2 nm can be observed (white arrows, dashed line and the corresponding height profile in Figure 4K). In a previous report, the AFM tip-induced formation of triangular WO_3 film with height of 2.1 nm on the WSe_2 single crystal was found when a bias voltage was applied under ambient condition.[31] The electric field induced electrochemical corrosion reaction was proposed to explain the formation of triangular WO_3. This kind of electrochemical corrosion reaction (also called photoetching) was usually found in electrolyte by using a tungsten halogen lamp as the light source.[27] Raman measurements (Figure 4E–H and M–P) further confirmed the formation of WO_3. As shown in Figure 4H,P, the Raman peaks at 822 cm^{-1} indicates the formation of hexagonal WO_3 after high power laser-induced

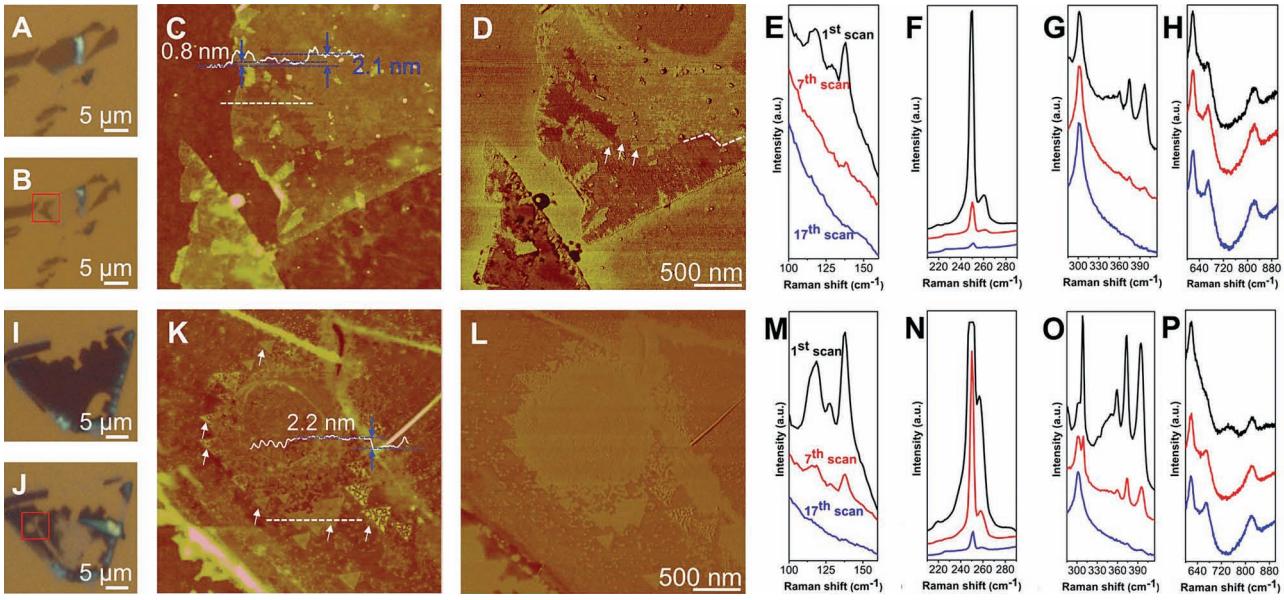

Figure 4. Optical images of 1L and 2L WSe_2 nanosheet before (A: 1L; I: 2L) and after (B: 1L; J: 2L) Raman characterization. (C) AFM height and (D) phase images of the red square area of 1L WSe_2 nanosheet shown in (B). The WO_3 parts give brighter contrast. Note the structures with 60° or 120° angles marked with white arrows and dashed lines in (D). Inset in (C) shows the height profile of the white dashed line. Raman spectra of 1L WSe_2 (E-H) and 2L WSe_2 (M–P) nanosheets in the range of (E and M) 100–160 cm^{-1}, (F and N) 210–290 cm^{-1}, (G and O) 285–415 cm^{-1} and (H and P) 600-900 cm^{-1} excited for long exposure time (200 s) and with high excitation power (5.1 mW) at the same spot after the 1st (black curves), 7th (red curves) and 17th (blue curve) Raman measurements. (K) AFM height and (L) phase images of the red square area of 2L WSe_2 nanosheet shown in (J). The WO_3 parts give brighter contrast. Note that the triangular structures marked with white arrows in (K). Inset in (K) shows the height profile of the corresponding white dashed line.

oxidation.[48] To our best knowledge, it is the first time to oxidize single- to few-layer WSe_2 nanosheets to form hexagonal WO_3 by using high power laser in ambient conditions. This indeed paves a facile and efficient way to produce thin-layer WO_3 with controlled crystal structure, dimension and location.

As shown in Figure 4F,N, the intensity of A_{1g} mode of 1L and 2L WSe_2 nanosheets decreased to 13% and 2% (for 1L), and 80% and 2% (for 2L) after the 7th and 17th Raman measurements, respectively. All typical Raman peaks of WSe_2 in the range of 100–415 cm^{-1} almost disappeared after the 17th measurement (Figure 4E–G and M–O), indicating that the WSe_2 nanosheets exposed to the laser spot was almost damaged with long exposure time and high laser power.

Similar phenomena were also observed in the 3L to 5L WSe_2 nanosheets (Figure S6 in SI). The Raman peaks appeared at 822, 822, 822, 811 and 807 cm^{-1} for 1L, 2L, 3L, 4L, and 5L WSe_2 nanosheets (**Figure 5**) after they were measured for 17 times (for 1L and 2L) and 12 times (for 3–5L), respectively. The peak around 810 cm^{-1} is attributed to the monoclinic structured WO_3 while the peak around 820 cm^{-1} is attributed to the hexagonal structured WO_3.[48,52] Therefore, the WO_3 converted from 1L to 3L WSe_2 nanosheets should be the hexagonal WO_3, while the WO_3 converted from 4L and 5L WSe_2 nanosheets should be the monoclinic WO_3. This can be further confirmed by AFM measurements (Figure S4–S6 in SI). The nanostructures with 60° or 120° angle at their edges were observed on 1L to 3L WSe_2 nanosheets, further confirming that the formed WO_3 is hexagonally structured. The height of these structures is ~2.2 nm, which is consistent with the triangular WO_3 fabricated on WSe_2 single crystal by the electric field-induced oxidation.[31] However, the irregular structures were found on 4L and 5L WSe_2 nanosheets (Figure S6E–H in SI).

Our aforementioned findings clearly prove that the WSe_2 thin layers are sensitive to the laser irradiation, and the micro-Raman spectroscopy measurement in the ambient conditions

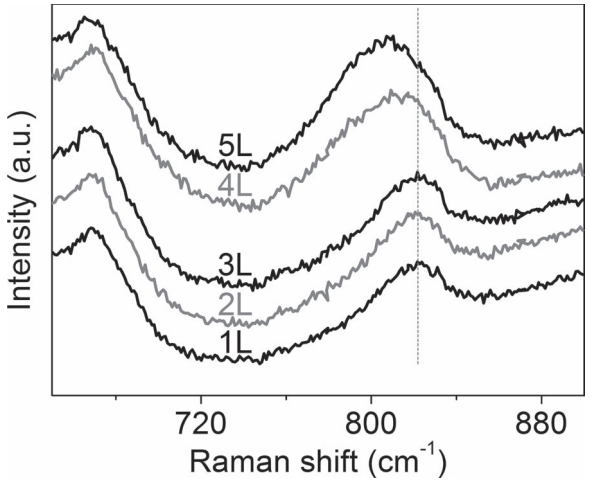

Figure 5. Raman spectra of 1L to 5L WSe_2 nanosheets after 17 times (for 1L and 2L) and 12 times (for 3L–5L) of Raman characterization in the range of 650–900 cm^{-1}. The spectra were excited by using a 532 nm laser with excitation power of 5.1 mW. The exposure time for each characterization is 200 s.

NANO MICRO small

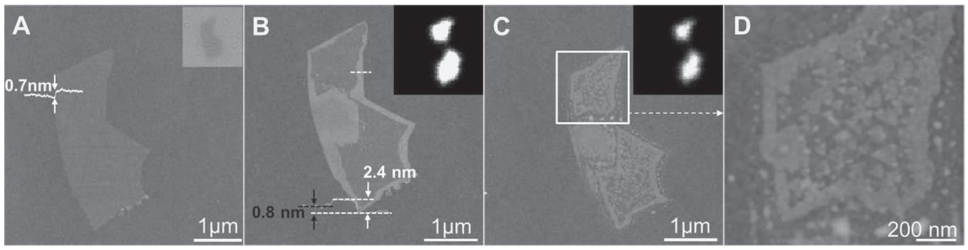

Figure 6. AFM images of 1L WSe_2 nanosheet before (A) and after the 1st (B) and 2nd (C) rounds of Raman mapping. Top-right insets: (A) the optical image, (B–C) the corresponding Raman mapping images of the 1L WSe_2 nanosheet. Bottom inset in (B) shows the height profile of the white dashed line. (D) AFM image of the white square in (C).

could also trigger the oxidation. Here, Raman mapping was conducted for the purpose of converting the thin-layer WSe_2 nanosheets to WO_3 and simultaneously probing the change of their crystal structures. **Figure 6**A,B show the AFM images of 1L WSe_2 nanosheet before and after Raman mapping in the spectral range of 200–270 cm^{-1}. It was reported that the defect-free vdW face of WSe_2 is inert towards the oxidation and corrosion.[30] As shown in Figure 6B, the oxidation starts from the edges of 1L WSe_2 nanosheet, which indicates the edges of mechanical-exfoliated WSe_2 nanosheet are highly defective. The height of the edges increased from 0.8 to 2.4 nm after Raman mapping, indicating the oxidation of WSe_2. The formed WO_3 film shows structures with 60° or 120° angle, indicating the hexagonal structure of WO_3, which is consistent with the Raman result. At this stage, the morphology of 1L WSe_2 in the central area keeps intact, indicating that the smooth, defect-free vdW face of WSe_2 prepared by the mechanical exfoliation is inert to the laser-induced oxidation. After the second round of Raman mapping, many triangular structures with height of 2.4 nm appeared in the WSe_2 nanosheet (Figure 6C,D), further confirming the formation of hexagonal structured WO_3 converted from the initial WSe_2 by the high power laser-induced oxidation.

Moreover, the oxidation of 2L WSe_2 nanosheet was also performed and simultaneously studied by using Raman mapping. **Figure 7**A shows the optical image of 2L WSe_2 nanosheet on 300 nm SiO_2 coated Si substrate. Figure 7B–E show the results of the 2L WSe_2 nanosheet after the 1st, 2nd, 3rd and 4th rounds of Raman mapping in the spectral range of 200–270 cm^{-1}, respectively. It is clearly seen that the Raman signal intensity of 2L WSe_2 nanosheet decreased as the Raman mapping cycles increased, indicating that more WO_3 was formed and less WSe_2 left with increased cycles of Raman mapping. The height of 2L WSe_2 nanosheet is 1.6 nm (Figure 7F). AFM measurement indicates the 2L WSe_2 nanosheet is more stable than the 1L WSe_2 nanosheet under high power laser irradiation. 1L WSe_2 nanosheet was damaged after 2 rounds of Raman mapping and only triangular WO_3 sheets left (Figure 6C,D), while some parts of WSe_2 with height of 1.6 nm were still found on the 2L WSe_2 nanosheet even after 4 rounds of Raman mapping (Figure 7G–H). However, the triangular WO_3 was also found

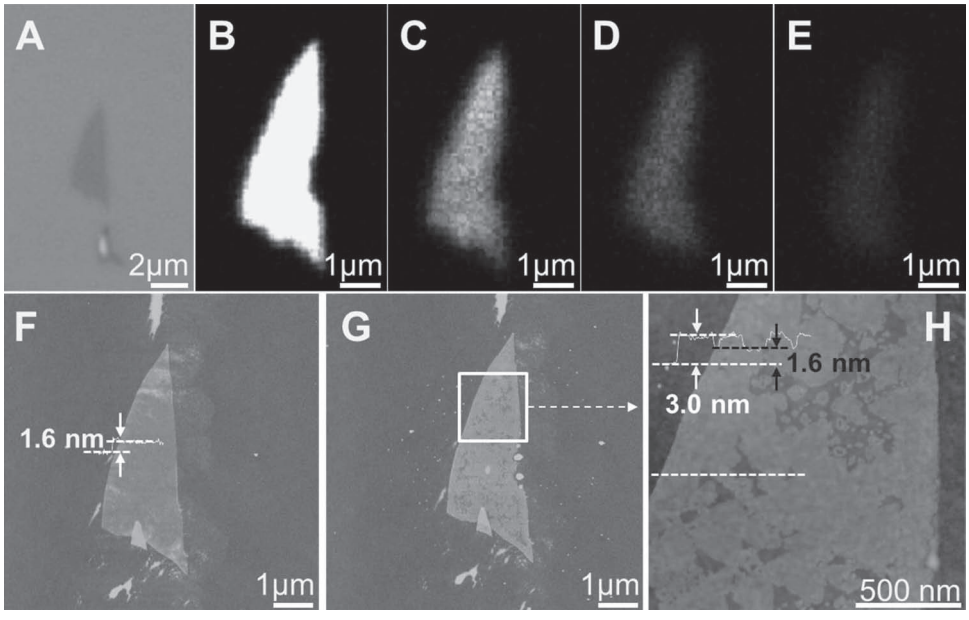

Figure 7. (A) Optical and (B–E) Raman mapping images of 2L WSe_2 nanosheet after the 1st, 2nd, 3rd and 4th rounds of Raman mapping. (F) AFM image of 2L WSe_2 nanosheet shown in (A). (G) AFM image of 2L WSe_2 nanosheet after the 4th round of Raman mapping in (E). (H) AFM image of the white square in (G). Inset: height profile of the white dashed line.

in the 2L WSe_2 nanosheet after 4 rounds of Raman mapping, whose height is ca. 3 nm (Figure 7H).

In order to study the electric properties of the thin-layer WSe_2 nanosheets, field-effect transistors (FETs) were fabricated based on the 1L and 3L WSe_2 nanosheets. Figure S7A and C in SI show the conductivity of 1L and 3L WSe_2 FETs, respectively. The recorded I_{ds}-V_g characteristic curve is typical of 1L WSe_2 FET with a p-type channel and a current On/Off ratio of 20 (Figure S7B in SI). Similarly, the 3L WSe_2 FET also showed the p-type doping characteristic with a higher current On/Off ratio of 400 (Figure S7D in SI). Since there are two kinds of WSe_2 single crystals, i.e., p-type and n-type, depending on the synthesis procedure,[28,56,57] our electric results of WSe_2 FETs indicate that the p-type single crystal of WSe_2 was used in this study.

In addition, the TaS_2 and $TaSe_2$ thin layers were also fabricated by the mechanical exfoliation method. The optical contrast of thin TaS_2 flake on 300 nm (Figure S8A) or 90 nm SiO_2 (Figure S8C) coated Si substrate is quite low. The thinnest TaS_2 nanosheet with thickness of ~2.1 nm, corresponding to 3 layers, is observed (Figure S8B,D). It is found that the thin-layer $TaSe_2$ nanosheet (Figure S9A) is very unstable and can be damaged by the light irradiation from a halogen lamp under an OM and lots of triangular nanostructures can be found (Figure S9B-D), which might be TaO_3.

3. Conclusion

In summary, single- and few-layer TMD nanosheets, such as WSe_2, TaS_2 and $TaSe_2$, were prepared on Si/SiO_2 substrate by the scotch tape-based mechanical exfoliation method. Raman measurements show the typical first order Raman peaks of WSe_2 together with some second order and the combinational modes. For the first time, a new Raman peak around 308 cm^{-1} was noticed except for the 1L WSe_2 nanosheet, which should be related to the interlayer interaction. Red shift of the A_{1g} mode and Raman peak around 308 cm^{-1} was observed as the layer number increased from 1L to 5L. The hexagonal-structured and monoclinic-structured WO_3 thin films were obtained during the local oxidation of WSe_2 nanosheets with layer numbers of 1L-3L and 4L-5L, respectively. While for the WSe_2 single crystal, the laser-burned hole was found. High power laser-induced oxidation of WSe_2 paves a facile and efficient way to produce thin-layer WO_3 with controlled crystal structure, dimension and location. In addition, the TaS_2 and $TaSe_2$ thin layers were also briefly characterized.

4. Experimental Section

Mechanical Exfoliation of WSe_2, TaS_2 and $TaSe_2$: Single crystals of WSe_2, TaS_2 and $TaSe_2$ were purchased from Nanoscience Instruments, Inc. (AZ, USA). Single- and few-layer WSe_2, TaS_2 and $TaSe_2$ sheets were isolated from the bulk single crystals and then deposited onto the freshly cleaned 300 nm or 90 nm SiO_2 coated Si substrates by using the scotch tape-based mechanical exfoliation method. The optical microscope (Eclipse LV100D, Nikon) was used to locate the single- and few-layer WSe_2, TaS_2 and $TaSe_2$ nanosheets. AFM (Dimension 3100 with Nanoscope IIIa controller, Veeco, CA, USA) was used to confirm the layer number by measuring the film thickness in tapping mode in air.

Raman Spectroscopy: Analysis of the single- and few-layer WSe_2 nanosheets by Raman spectroscopy was carried out on a Renishaw inVia Raman microscope. All spectra were excited at room temperature with laser light ($\lambda = 532$ nm) and recorded through the 100× objective. A 2400-lines/mm grating provided a spectral resolution of ~1 cm^{-1}. Raman mapping was performed on a WITec CRM200 confocal Raman microscopy system by using the 488 nm laser with an excitation power of 0.7 mW and integration time of 0.05 s. The Raman band of a silicon wafer at 520 cm^{-1} was used as a reference to calibrate the spectrometer. The power level of laser was measured by a handheld laser power meter (LaserCheck, Coherent Inc., USA) through the 100× objective. To get comparable signals, the Raman spectra of WSe_2 single crystal shown in Figure 1A with excitation power of 0.28, 0.58 and 2.6 mW are accumulated for 5 times with 10 s per accumulation.

Fabrication and Characterization of WSe_2 FETs: The source and drain electrodes of WSe_2 FET devices were fabricated by the traditional photolithography. The 5 nm Ti/50 nm Au source-drain electrodes were deposited by using the electron beam evaporator. After removal of photoresist, the electrical properties of the few layer WSe_2 FETs were tested by the Keithley 4200 semiconductor characterization system in air at room temperature.

Supporting Information

Supporting Information is available from the Wiley Online Library or from the author.

Acknowledgements

This work was supported by Singapore National Research Foundation under CREATE programme: Nanomaterials for Energy and Water Management, and NTU under the Start-Up Grant (M4080865.070.706022) in Singapore. T. Yu acknowledges the grant of NTU-SUG M4080513.

[1] K. S. Novoselov, A. K. Geim, S. V. Morozov, D. Jiang, Y. Zhang, S. V. Dubonos, I. V. Grigorieva, A. A. Firsov, *Science* **2004**, *306*, 666.
[2] K. S. Novoselov, D. Jiang, F. Schedin, T. J. Booth, V. V. Khotkevich, S. V. Morozov, A. K. Geim, *Proc. Natl. Acad. Sci. USA* **2005**, *102*, 10451.
[3] A. K. Geim, K. S. Novoselov, *Nat. Mater.* **2007**, *6*, 183.
[4] X. Huang, Z. Y. Yin, S. X. Wu, X. Y. Qi, Q. Y. He, Q. C. Zhang, Q. Y. Yan, F. Boey, H. Zhang, *Small* **2011**, *7*, 1876.
[5] X. Huang, X. Y. Qi, F. Boey, H. Zhang, *Chem. Soc. Rev.* **2012**, *41*, 666.
[6] H. Li, Z. Y. Yin, Q. Y. He, X. Huang, G. Lu, D. W. H. Fam, A. I. Y. Tok, Q. Zhang, H. Zhang, *Small* **2012**, *8*, 63.
[7] H. Li, G. Lu, Z. Yin, Q. He, H. Li, Q. Zhang, H. Zhang, *Small* **2012**, *8*, 682.
[8] Z. Y. Yin, H. Li, L. Jiang, Y. M. Shi, Y. H. Sun, G. Lu, Q. Zhang, X. D. Chen, H. Zhang, *ACS Nano* **2012**, *6*, 74.
[9] Z. Zeng, Z. Yin, X. Huang, H. Li, Q. He, G. Lu, F. Boey, H. Zhang, *Angew. Chem. Int. Ed.* **2011**, *50*, 11093.

[10] J. N. Coleman, M. Lotya, A. O'Neill, S. D. Bergin, P. J. King, U. Khan, K. Young, A. Gaucher, S. De, R. J. Smith, I. V. Shvets, S. K. Arora, G. Stanton, H. Y. Kim, K. Lee, G. T. Kim, G. S. Duesberg, T. Hallam, J. J. Boland, J. J. Wang, J. F. Donegan, J. C. Grunlan, G. Moriarty, A. Shmeliov, R. J. Nicholls, J. M. Perkins, E. M. Grieveson, K. Theuwissen, D. W. McComb, P. D. Nellist, V. Nicolosi, *Science* **2011**, *331*, 568.
[11] C. Lee, Q. Y. Li, W. Kalb, X. Z. Liu, H. Berger, R. W. Carpick, J. Hone, *Science* **2010**, *328*, 76.
[12] K. F. Mak, C. Lee, J. Hone, J. Shan, T. F. Heinz, *Phys. Rev. Lett.* **2010**, *105*, 136805.
[13] A. Splendiani, L. Sun, Y. B. Zhang, T. S. Li, J. Kim, C. Y. Chim, G. Galli, F. Wang, *Nano Lett.* **2010**, *10*, 1271.
[14] M. M. Benameur, B. Radisavljevic, J. S. Heron, S. Sahoo, H. Berger, A. Kis, *Nanotechnology* **2011**, *22*, 125706.
[15] B. Radisavljevic, A. Radenovic, J. Brivio, V. Giacometti, A. Kis, *Nat. Nanotechnol.* **2011**, *6*, 147.
[16] H. S. S. R. Matte, A. Gomathi, A. K. Manna, D. J. Late, R. Datta, S. K. Pati, C. N. R. Rao, *Angew. Chem. Int. Ed.* **2010**, *49*, 4059.
[17] R. J. Smith, P. J. King, M. Lotya, C. Wirtz, U. Khan, S. De, A. O'Neill, G. S. Duesberg, J. C. Grunlan, G. Moriarty, J. Chen, J. Wang, A. I. Minett, V. Nicolosi, J. N. Coleman, *Adv. Mater.* **2011**, *23*, 3944.
[18] a) S. Wu, Z. Zeng, Q. He, Z. Wang, S. J. Wang, Y. Du, Z. Yin, X. Sun, W. Chen, H. Zhang, *Small* **2012**, *8*, 2264; b) Q. Y. He, Z. Y. Zeng, Z. Y. Yin, H. Li, S. X. Wu, X. Huang, H. Zhang, *Small* **2012**, *8*, 2994; c) J. Q. Liu, Z. Y. Zeng, X. H. Cao, G. Lu, L. H. Wang, Q. L. Fan, W. Huang, H. Zhang, *Small* **2012**, *8*, 3517; d) W. J. Zhou, Z. Y. Yin, Y. P. Du, X. Huang, Z. Y. Zeng, Z. X. Fan, H. Liu, J. Y. Wang, H. Zhang, *Small*, DOI: 10.1002/smll.201201161; e) Z. Y. Yin, Z. Y. Zeng, J. Q. Liu, Q. Y. He, P. Chen, H. Zhang, *Small*, DOI: 10.1002/smll. 201201940.
[19] K.-G. Zhou, N.-N. Mao, H.-X. Wang, Y. Peng, H.-L. Zhang, *Angew. Chem. Int. Ed.* **2011**, *50*, 10839.
[20] Z. Y. Zeng, T. Sun, J. X. Zhu, X. Huang, Z. Y. Yin, G. Lu, Z. X. Fan, Q. Y. Yan, H. H. Hng, H. Zhang, *Angew. Chem. Int. Ed.* **2012**, *51*, 9052.
[21] C. Chiritescu, D. G. Cahill, N. Nguyen, D. Johnson, A. Bodapati, P. Keblinski, P. Zschack, *Science* **2007**, *315*, 351.
[22] A. Mavrokefalos, N. T. Nguyen, M. T. Pettes, D. C. Johnson, L. Shi, *Appl. Phys. Lett.* **2007**, *91*, 171912.
[23] S. W. Kim, J. M. Zuo, N. T. Nguyen, D. C. Johnson, D. G. Cahill, *J. Mater. Res.* **2008**, *23*, 1064.
[24] N. T. Nguyen, P. A. Berseth, Q. Lin, C. Chiritescu, D. G. Cahill, A. Mavrokefalos, L. Shi, P. Zschack, M. D. Anderson, I. M. Anderson, D. C. Johnson, *Chem. Mater.* **2010**, *22*, 2750.
[25] D. G. Mead, J. C. Irwin, *Can. J. Phys.* **1977**, *55*, 379.
[26] H. J. Lewerenz, A. Heller, F. J. Disalvo, *J. Am. Chem. Soc.* **1980**, *102*, 1877.
[27] R. Tenne, A. Wold, *Appl. Phys. Lett.* **1985**, *47*, 707.
[28] A. Jakubowicz, D. Mahalu, M. Wolf, A. Wold, R. Tenne, *Phys. Rev. B* **1989**, *40*, 2992.
[29] D. Mahalu, M. Peisach, W. Jaegermann, A. Wold, R. Tenne, *J. Phys. Chem.* **1990**, *94*, 8012.
[30] D. Mahalu, L. Margulis, A. Wold, R. Tenne, *Phys. Rev. B* **1992**, *45*, 1943.
[31] M. Bohmisch, F. Burmeister, J. Boneberg, P. Leiderer, *Appl. Phys. Lett.* **1996**, *69*, 1882.
[32] P. Salvador, A. M. Chaparro, A. Mir, *J. Phys. Chem.* **1996**, *100*, 760.
[33] D. Teweldebrhan, V. Goyal, A. A. Balandin, *Nano Lett.* **2010**, *10*, 1209.
[34] J. Zhang, Z. P. Peng, A. Soni, Y. Y. Zhao, Y. Xiong, B. Peng, J. B. Wang, M. S. Dresselhaus, Q. H. Xiong, *Nano Lett.* **2011**, *11*, 2407.
[35] a) K. Ariga, T. Mori, J. P. Hill, *Adv. Mater.* **2012**, *24*, 158; b) J. H. Lee, J. P. Singer, E. L. Thomas, *Adv. Mater.* **2012**, *24*, 4782; c) H. D. Espinosa, T. Filleter, M. Naraghi, *Adv. Mater.* **2012**, *24*, 2805.
[36] K. M. F. Shahil, M. Z. Hossain, D. Teweldebrhan, A. A. Balandin, *Appl. Phys. Lett.* **2010**, *96*, 153103.
[37] K. M. F. Shahil, M. Z. Hossain, V. Goyal, A. A. Balandin, *J. Appl. Phys.* **2012**, *111*, 054305.
[38] C. X. Cong, T. Yu, K. Sato, J. Z. Shang, R. Saito, G. F. Dresselhaus, M. S. Dresselhaus, *ACS Nano* **2011**, *5*, 8760.
[39] C. X. Cong, T. Yu, H. M. Wang, *ACS Nano* **2010**, *4*, 3175.
[40] C. Lee, H. Yan, L. E. Brus, T. F. Heinz, J. Hone, S. Ryu, *ACS Nano* **2010**, *4*, 2695.
[41] C. X. Cong, T. Yu, R. Saito, G. F. Dresselhaus, M. S. Dresselhaus, *ACS Nano* **2011**, *5*, 1600.
[42] E. Galun, H. Cohen, L. Margulis, A. Vilan, T. Tsirlina, G. Hodes, R. Tenne, M. Hershfinkel, W. Jaegermann, K. Ellmer, *Appl. Phys. Lett.* **1995**, *67*, 3474.
[43] S. K. Srivastava, B. N. Avasthi, *J. Mater. Sci.* **1985**, *20*, 3801.
[44] C. Sourisseau, F. Cruege, M. Fouassier, M. Alba, *Chem. Phys.* **1991**, *150*, 281.
[45] G. L. Frey, R. Tenne, M. J. Matthews, M. S. Dresselhaus, G. Dresselhaus, *Phys. Rev. B* **1999**, *60*, 2883.
[46] T. Sekine, M. Izumi, T. Nakashizu, K. Uchinokura, E. Matsuura, *J. Phys. Soc. Jpn.* **1980**, *49*, 1069.
[47] T. Sekine, T. Nakashizu, K. Toyoda, K. Uchinokura, E. Matsuura, *Solid State Commun.* **1980**, *35*, 371.
[48] M. F. Daniel, B. Desbat, J. C. Lassegues, B. Gerand, M. Figlarz, *J. Solid State Chem.* **1987**, *67*, 235.
[49] D. Y. Lu, J. Chen, S. Z. Deng, N. S. Xu, W. H. Zhang, *J. Mater. Res.* **2008**, *23*, 402.
[50] Y. Baek, K. Yong, *J. Phys. Chem. C* **2007**, *111*, 1213.
[51] K. Kalantar-zadeh, A. Vijayaraghavan, M. H. Ham, H. D. Zheng, M. Breedon, M. S. Strano, *Chem. Mater.* **2010**, *22*, 5660.
[52] C. Santato, M. Odziemkowski, M. Ulmann, J. Augustynski, *J. Am. Chem. Soc.* **2001**, *123*, 10639.
[53] Z. Zheng, B. Yan, J. Zhang, Y. You, C. T. Lim, Z. Shen, T. Yu, *Adv. Mater.* **2008**, *20*, 352.
[54] C. V. Ramana, S. Utsunomiya, R. C. Ewing, C. M. Julien, U. Becker, *J. Phys. Chem. B* **2006**, *110*, 10430.
[55] Y. Y. Wang, Z. H. Ni, Z. X. Shen, H. M. Wang, Y. H. Wu, *Appl. Phys. Lett.* **2008**, *92*, 043121.
[56] R. Spah, U. Elrod, M. Luxsteiner, E. Bucher, S. Wagner, *Appl. Phys. Lett.* **1983**, *43*, 79.
[57] L. C. Upadhyay, J. J. Loferski, A. Wold, W. Giriat, R. Kershaw, *J. Appl. Phys.* **1968**, *39*, 4736.

Received: November 23, 2012
Published online: January 6, 2013